Electrolyte Stability and Discharge Products of an Ionic-Liquid-based Li-O_2 Battery Revealed by Soft X-Ray Emission Spectroscopy

Aline Léon[1], Andy Fiedler[2], Monika Blum[3,4], Wanli Yang[4], Marcus Bär[5,6,7], Frieder Scheiba[2], Helmut Ehrenberg[2], Clemens Heske[1,3,8], and Lothar Weinhardt[1,3,8]*

1) Institute for Photon Science and Synchrotron Radiation (IPS), Karlsruhe Institute of Technology (KIT), Hermann-von-Helmholtz-Platz 1, 76344 Eggenstein-Leopoldshafen, Germany

2) Institute for Applied Materials (IAM), Karlsruhe Institute of Technology (KIT), Hermann-von-Helmholtz-Platz 1, 76344 Eggenstein-Leopoldshafen, Germany

3) Department of Chemistry and Biochemistry, University of Nevada, Las Vegas (UNLV), NV 89154-4003, USA

4) Advanced Light Source (ALS), Lawrence Berkeley National Laboratory, Berkeley, California 94720, United States

5) Department of Interface Design, Helmholtz-Zentrum Berlin für Materialien und Energie GmbH (HZB), Albert-Einstein-Str. 15, 12489 Berlin, Germany

6) Helmholtz-Institute Erlangen-Nürnberg for Renewable Energy (HI ERN), Albert-Einstein-Str. 15, 12489 Berlin, Germany

7) Department of Chemistry and Pharmacy, Friedrich-Alexander-Universität Erlangen-Nürnberg, Egerlandstr. 3, 91058 Erlangen, Erlangen, Germany

8) Institute for Chemical Technology and Polymer Chemistry (ITCP), Karlsruhe Institute of Technology (KIT), Engesserstr. 18/20, 76128 Karlsruhe, Germany

* Corresponding author: aline.leon@eifer.org

Abstract

We investigate the electrolyte stability and discharge products of an ionic-liquid-based Li-O_2 battery through soft x-ray emission spectroscopy (XES) experiments, which offer unique site specificity for detecting subtle changes in the local nitrogen and oxygen environment. We benchmark the valence electronic structures of the molecules composing the electrolyte, namely the solvent PP13(TFSI), the salt LiTFSI, and the PP13 cation. Then, the transformation of the electrolyte is shown using cathodes stopped at different discharge and charge stages. We provide experimental evidence that the nitrogen site of the salt is unstable during electrochemical operation. The chemical environment of the nitrogen atoms is gradually changed during the electrochemical cycle, indicating a breaking of S-N bonds. The ionic liquid solvent remains mostly as an ion pair, but some decomposition into PP13 cations and TFSI anions cannot be ruled out. Our results and detailed analysis also show that the discharge products in our cell consist of lithium peroxide with some amount of hydroxide; however, no carbonate is observed.

1. Introduction

Li-O_2 battery technology, with a potential energy density of 500 Wh/kg,[1] has been considered for the next generation of rechargeable batteries. However, low capacity, poor rate capability, low round-trip efficiency, and short cycle life are technical limitations[2,3] inherent to this battery caused by the special chemical environment and the complex chemistry of gaseous, liquid, and solid reaction products. The practical barriers and the complicated reactions require advanced characterizations, especially elemental- and site-sensitive (ideally *in situ/operando*) spectroscopy, to clarify the complicated chemistry associated with critical challenges on both the electrode and the electrolyte.[4,5]

The oxygen electrode is usually made of a three-dimensional network structure that features high surface area and excellent electronic conductivity. However, the electrode undergoes passivation during the discharge process because of the formation of poorly conducting Li_2O_2 on the carbon cathode.[6] Therefore, novel approaches are developed based on synthesizing advanced nanostructured carbon electrodes,[7,8,9] coating the existing carbon cathodes with non-carbon materials,[10,11,12] or designing a complete carbon-free electrode[13,14,15] to minimize the degradation of the oxygen electrode.

The electrolyte, based on a solvent and a lithium salt, is known to degrade gradually during the discharge and charge process.[16] At first, organic carbonate-based solvents were widely used in Li-O_2 cells. However, they were decomposing irreversibly during the electrochemical reaction. The side-reaction products were found to be lithium carbonate and lithium alkyl carbonate.[17] Thus, dimethyl sulfoxide, as well as ether-based solvents (i.e., dimethyl ether, diglyme, tetraglyme), were investigated, but low round-trip energy efficiency and long-term stability remain an issue with both solvents under the presence of Li_2O_2.[18,19,20]

The most common salts used are $LiPF_6$, $LiClO_4$, $LiN(SO_2CF_3)_2$, $LiNO_3$, and LiBr. The electrochemical performance was found to be affected by the salt concentration and the reactivity of the anion towards lithium peroxide formed during the discharge reaction. [21,22,23] A practically viable electrolyte system is yet to be found for Li-O_2 batteries, and different pathways are currently explored, either by modifying the solvents with additives[24] or by using ionic-liquid-based electrolytes[25,26] or solid state ones.[27]

Clearly, an optimization of the Li-O_2 system is necessary that requires additional understanding of the electrochemical and chemical reactions on the atomic/molecular level. Here, based on our previous results that soft x-ray emission spectroscopy (XES) can clearly differentiate the four key discharge products of non-aqueous Li-O_2 batteries, namely Li_2O_2, Li_2O, Li_2CO_3, and LiOH,[28] we employ the site specificity at the O and N K edges of XES to probe the decomposition mechanism of the electrolyte and the discharge products during the initial electrochemical cycle of the ionic-liquid-based Li-O_2 system. In this system, metallic lithium is used as anode, PP13(TFSI) [1-Methyl-1-Propylpiperidinium bis (trifluorosulfonyl)imide] as solvent, LiTFSI (lithium trifluorosulfonylimide) as salt (0.5 M), and a porous carbon electrode as cathode.

2. Materials and Methods

2.1. References and samples

As references, we investigated the gas diffusion layer (GDL) sheet (porous carbon cathode, as received), the PP13(TFSI) solvent, the Li(TFSI) salt (as received), and the electrolyte (PP13(TFSI) + 0.5M LiTFSI) (as prepared). The reference powders were pressed onto carbon tape and mounted on a sample holder. Liquid samples were impregnated on a piece of the GDL before being placed onto carbon tape.

Four samples, two during the discharge and two during the charge reaction, were prepared using the electrochemical cell described below. All parameters for the preparation of the four samples were kept constant, except for the potential at which the reaction was stopped. Potentials of 2.5 and 1.5 V were selected for the discharge reaction and labeled V_1 and V_2, respectively. For the charge process, the electrochemical reaction was stopped at V_3 = 3.5 V and V_4 = 4.5 V. The potentiostat was programmed to charge or discharge the cell to the defined potential and hold this potential for 24 hours. Thereafter, the cell was disassembled inside an Ar-purged glove box, the cathode removed and mounted without further treatment on a sample holder using carbon tape. To avoid any air exposure, the sample holder was inserted into a transportable vacuum system and sealed under inert atmosphere inside the glove box. The transportable vacuum system was connected to the load lock of the synchrotron endstation and evacuated before transferring the sample holder into the analysis chamber.

2.2. Electrochemical set-up

For the current Li-O_2 electrochemical experiments, a lithium metal (Alfa Aesar, purity 99.9%) anode of 12 mm diameter was mounted on a titanium collector. The electrolyte consisted of LiTFSI salt (Alfa Aesar, 99.95% purity) dissolved in PP13(TFSI) ionic liquid solvent (IoLiTec, 99% purity and 48 ppm water). A 3 mm diameter piece of glass fiber separator (Whatman) was impregnated with 150 to 200 µl of the electrolyte and placed on top of the anode. A 7 mm diameter cathode was punched from a Gas Diffusion Layer (GDL) sheet (Freudenberg, H2315/C_2 – microporous layer, 90% porosity). The cathode and anode were dried under vacuum for 12 hours before introduction into an Ar-filled glove box (water and oxygen concentrations below 1 ppm).

The cell was first sealed in the Ar-filled glove box and connected outside to a high purity gas line (argon or oxygen) equipped with mass flow controllers for a controlled circulation of the gas through the cathode. The cell was flushed with argon, and then an oxygen flow of 10 sccm

was applied for one hour at open circuit voltage (OCV) of 3.3 V. Thereafter, cyclic voltammetry tests were carried out with a SP-150 potentiostat (BioLogic) at room temperature and a scan rate of 10 mV/s. The cyclic voltammograms were acquired by starting at OCV, scanning first to 1.5 V, and subsequently to 4.5 V before returning to the OCV. All potentials in this paper are referenced to the Li^+/Li couple.

2.3. XES spectra acquisition

The experiments were performed at the undulator beamline 8.0.1.2 of the Advanced Light Source, Lawrence Berkeley National Laboratory, using the SALSA endstation[29] equipped with a high-transmission soft x-ray spectrometer.[30] The pressure during the experiments was $< 1 \times 10^{-8}$ mbar, and the estimated spot size 150 (h) × 30 (v) μm^2.

XES spectra were acquired with non-resonant excitation at the N and O K edge, using excitation energies of 433.7 and 547.4 eV, respectively. To minimize beam damage, the XES spectra were recorded while constantly scanning the sample with a speed of 50 μm/s across an area of 1.2 × 1.2 mm^2 (corresponding to an exposure time of ~ 0.6 seconds for any given spot on the sample). The reference spectra of the different components involved were normalized to the maximum of the signal. To follow the evolution of the reaction at different potentials, the spectra were normalized to the integrated area of the spectrum.

The excitation energy scale was calibrated at the N and O K edge by measuring an XAS spectrum of N_2 gas[31] and TiO_2 (anatase),[32] respectively. The energy scale of the emission energy was calibrated using the elastically scattered Rayleigh lines.

3. Results and discussion

3.1. Cyclic voltammetry

Figure 1 displays the cyclic voltammetry measurements under argon flow (green, one cycle) and two consecutive cycles under oxygen flow (red). The first scan was run under an inert atmosphere of argon to provide a background voltammogram. As can be seen, no appreciable current is observed over the full potential range of the oxygen reduction reaction (ORR) and oxygen evolution reaction (OER). The first cycle under oxygen indicates that the ORR starts at a potential of 2.5 V and reaches a maximum current of 80 μA at 1.5 V. On the reverse scan, the OER starts around 3.2 V and is smeared out over a large potential range (up to, at least, 4.5 V). The second oxygen cycle shows a similar redox process, with a decrease of the discharge capacity compared to the first cycle, indicating a partial passivation of the electrode surface or presence of side reaction products with the electrolyte.

3.2. Valence electronic structure of solvent and salt, as seen at the N K edge

We first determine the signature of the electrolyte at the N K edge by analyzing the spectra of the different molecules involved, namely PP13(TFSI), LiTFSI, and PP13. Figure 2 displays the measured nitrogen K XES spectra of the electrolyte, Li(TFSI), and PP13(TFSI). The N K-edge spectrum of LiTFSI represents the local partial density of states (PDOS) of the TFSI anion. The spectrum of the salt is described by a prominent peak at 393.5 eV, two weak features at ~386.4 eV and ~381.7 eV, a low-energy shoulder at ~391.5 eV, and a high-energy shoulder at ~395.6 eV. This is in agreement with the derived N K XES spectrum of TFSI published by Kanai et al.[33]

The spectrum of the solvent consists of emission from both the PP13 cation and the TFSI anion. It is characterized by a main peak at 393.5 eV accompanied by a high-energy shoulder at ~ 395.2 eV, a low-energy shoulder at ~ 390.2 eV, and some weak features at ~383.7 and ~381.7 eV. The spectral contribution of the N atom in the PP13 cation can now be obtained by computing the difference between the spectra of PP13(TFSI) and LiTFSI (the latter weighted by a factor of 0.5). As can be seen, the spectral contribution of the PP13 cation is defined by a

peak at ~395 eV [giving rise to the PP13(TFSI) high-energy shoulder at ~ 395.2 eV], by a broad peak on the low-energy side centered at ~ 391.5 eV, and a weak feature at ~ 383.7 eV.

The spectrum of the electrolyte is expected to be mostly a combination of the solvent and salt spectra. Indeed, it mainly consists of a peak related to the TFSI molecule at 393.5 eV and high- and low-energy shoulders related to the PP13 cation (at ~ 395 and ~ 391.5 eV, respectively). Interestingly, small spectral lineshape enhancements are observed between 381 and 385 eV, indicating that there may be internal molecular interactions in the electrolyte composition.

3.3. Stability of nitrogen site in the solvent and salt molecules

In the previous section, we have shown that the two molecules in the electrolyte feature a specific valence electronic structure at the nitrogen site, which can be probed and distinguished with N K XES. In the following, we use this site specificity to follow the evolution of nitrogen atoms from the salt and the solvent at different stages of the reaction during the first cycle of the cyclic voltammogram. Figure 3 shows the N K XES spectra of the electrolyte, as prepared and as stopped at potentials V_1, V_2, V_3, and V_4. The spectra were normalized to the integrated area of the spectrum. As shown in Figure S1, we find that the spectral shapes change slightly, and that the intensity of the prominent TFSI-related peak at 393.5 eV decreases during the course of the first cycle from OCV to V_4, indicating a change in the local chemical environment of (some of) the nitrogen atoms. In order to clarify the mechanism, the experimental data at different stages of the reaction were fitted by a linear combination of the two components PP13(TFSI) and LiTFSI. The composition evolution of these components during the discharge and the following charge process is shown in Figure 4. During discharge, the percentage of LiTFSI decreases already at potential V_1, from 60% to 18%. During charge, it further decreases, reaching 3% at the end of the charge. This clearly indicates that the nitrogen site of the salt is unstable when applying a voltage different from the OCV. Further nitrogen atoms are gradually removed from the TFSI anion during the electrochemical cycle, indicating, most probably, a

breaking of the S-N bond in the anion. The observed decomposition of the anion is very similar to what has been observed with N-methyl-N-propyl-pyrrolidinium TFSA (P13TFSA)[34] and calculated for N, N-propyl-ethyl-pyrrolidinium (P13TFSI)[35], where the TFSA and TFSI anions were shown to be less stable against reduction than the P13 cation. The decomposition of the solvent is partially in agreement with the quantum molecular dynamics simulation by Nishino et al.[36], who conclude that the PP13(TFSI) molecule behaves as a complex without spontaneous dissociation of the PP13(TFSI) ion pair. We cannot currently make conclusions about the remaining fragments, but our results and analysis unambiguously show that the nitrogen site of the TFSI anion of the salt and solvent is highly unstable under the reduction of oxygen and decomposition of Li_2O_2.

3.4. Discharge products

During the discharge, it is proposed that only lithium peroxide is formed.[2,18] However, depending on the electrolyte, it has been shown that other side-products like lithium carbonate, lithium hydroxide, and/or lithium fluoride can also be present.[16, 19] These side-products could be due to decomposition of the electrolyte or a chemical reaction with the carbon cathode. Here, we characterized the discharge products by analyzing the O K XES spectra of the cathode obtained at potential V_2. As the cathode was measured *ex situ* without further treatment, the carbon cathode, the electrolyte, and the discharge products contribute to the oxygen signal at this voltage. Figure 5a displays the O K XES spectra of the as-received carbon cathode (GDL), the as-prepared electrolyte, and the cathode (V_2) after being kept at V_2 = 1.5 V for 24 hours. As can be seen, the oxygen contribution from the carbon cathode is very small (approx. 1/70) compared to the electrolyte. The O K XES spectrum of the electrolyte is dominated by two main peaks, at ~523 and ~527 eV. The spectrum reflects the local PDOS of the four oxygen atoms of the TFSI molecule. The spectrum of the cathode at potential V_2 is very similar to the

one of the electrolyte, as displayed in Figure S2, suggesting the formation of very small amounts of O-containing discharge products.

To quantify the different oxygen contributions, the spectrum is fitted with three components, as described in the following. First, we performed a three-component fit, using the spectra of Electrolyte, GDL, and lithium peroxide.[28] The result of the fit and the corresponding magnified residual (x10, labelled V_2-fit residual) is shown in Figure 5b, top. The fit gives a good description of the spectrum with the following spectral weights: 1.5% GDL, 95.0% electrolyte, and 3.5% lithium peroxide. A three-component analysis with GDL, electrolyte, and lithium carbonate or lithium hydroxide *alone* fails to describe properly the rising shoulder and the highest energy side peak of the O K spectrum at the potential V_2. The respective spectra of Li_2O_2, Li_2CO_3, and LiOH are shown at the bottom of Fig. 5b for comparison. Therefore, we conclude that the dominant discharge product is Li_2O_2 and the spectral weight is similar to the amount expected for the time of reaction from the analysis of the first reduction peak.

Finally, in order to test whether the three-component description can still be significantly improved, the V_2 spectrum was analyzed by a *four*-component analysis, i.e., using GDL, electrolyte, Li_2O_2, and either Li_2CO_3 or LiOH as fit functions. The better agreement is obtained with LiOH (1.5% GDL, 93.4% electrolyte, 2.9% Li_2O_2, and 2.2% LiOH), as seen from the magnified residual labeled "adding LiOH (x10)", compared to the case where Li_2CO_3 is added (magnified residual labeled "adding Li_2CO_3 (x10)").

Therefore, we summarize that the main O-containing discharge product is Li_2O_2, with some lithium hydroxide also being present. However, based on our spectroscopic results, there is no significant amount of lithium carbonate formed during the discharge reaction. The presence of LiOH in the ionic-liquid-based electrolyte would be in accordance with a recent microscopy study[37] that shows the presence of LiOH crystallites, the amount of which depending on both the concentration of LiTFSI and the storage time of the discharged electrodes. Therefore, the

presence of LiOH is mostly at the origin of the electrodes surface passivation of the electrodes and by that explains the decrease of the discharge capacity observed in the second reaction cycle.

Using XES, each of the compounds shows features of clearly distinguishable spectral shape that will allow *in-situ* and *operando* measurements in the future. As an outlook, Figure 6 presents a schematic view of the novel flow-through electrochemical cell that represents a first step towards *in-situ* and *operando* XES measurements; additional scanning capabilities will be required to avoid the beam-damage effects reported in the manuscript by Léon et al.[28]

4. Conclusions

In this work, we used the site specificity of XES and a novel electrochemistry cell to probe the electrolyte and discharge products of an ionic-liquid-based Li-O_2 battery. We determined the valence electronic structure of PP13(TFSI), TFSI, and PP13 molecules at the N and O K edges. We observe that the spectral shapes change slightly and the chemical environment of some of the nitrogen atoms is significantly modified during the first discharge/charge cycle, suggesting a decomposition of the salt. The TFSI anion is found to be unstable at the nitrogen atom, while the ionic-liquid solvent appears to remain as an ion pair. Additionally, the O K edge XES spectra show that lithium peroxide and a small amount of lithium hydroxide are formed as discharge products; however, the formation of lithium carbonate cannot be observed.

There are no conflicts to declare

Acknowledgments

We acknowledge D. Kuntz (KIT – TEC) for the production of the electrochemical test cell. M. Bär thanks the Impuls und Vernetzungsfonds of the Helmholtz Association for funding (VH-NG-423). This research used resources of the Advanced Light Source, which is a DOE Office

of Science User Facility under contract no. DE-AC02-05CH11231, and contributes to the research performed at CELEST (Center for Electrochemical Energy Storage Ulm-Karlsruhe).

References

1. Bruce, P. G; Freunberger, S. A; Hardwick, L. J; Tarascon, J. M. Li-O_2 and Li-S batteries with high-energy storage *Nature Mat.* **2011**, *11*, 19-29.
2. Grande, L.; Paillard, E.; Hassoun, J.; Park, J. B.; Lee, Y. J.; Sun, Y. K.; Passerini, S.; Scrosati, B. The lithium/air battery: still an emerging system or a practical reality? *Adv. Mater.* **2015**, *27*, 784-800.
3. Shao, Y.; Ding, F.; Xiao, J.; Zhang, J.; Xu, W.; Park, S.; Zhang, J.G.; Wang, Y.; Liu, J. Making Li-air batteries rechargeable: material challenges *Adv. Funct. Mater*. **2013**, *23*, 987-1004.
4. Jung, K. N.; Kim, J.; Yamauchi, Y.; Park, M. S.; Lee, J. W.; Kim, J. H. Rechargeable lithium-air batteries: a perspective on the development of oxygen electrodes *J. Mater. Chem. A* **2016**, *4*, 14050-14068.
5. Li, Y.; Wang, X.; Dong, S.; Chen, X.; Cui, G. Recent advances in non-aqueous electrolyte for rechargeable Li-O_2 batteries *Adv. Energy. Mater.* **2016**, *6*, 1600751.
6. Albertus, P.; Girishkumar, G.; McCloskey, B.; Sanchez-Carrera, R.S.; Kozinsky, B.; Christensen, J.; Luntz, A.C. Identifying capacity limitations in the Li/oxygen battery using experiments and modeling *J. Electrochem. Soc.* **2011**, *158*, A343-A351.
7. Mitchell, R. R.; Gallant, B. M.; Thompson, C.V.; Shao-Horn, Y. All-carbon-nanofiber electrodes for high-energy rechargeable Li-O_2 batteries *Energy Environ. Sci.* **2011**, *4*, 2952-2958.

8. Li, Q.; Cao, R.; Cho, J.; Wu, G. Nanostructured carbon-based cathode catalysts for non-aqueous lithium-oxygen batteries *Phys. Chem. Chem. Phys.* **2014**, *16*, 13568-13582.
9. Jung, C. Y.; Zhao, T. S.; Zeng, L.; Tan, P. Vertically aligned carbon nanotube-ruthenium dioxide core-shell cathode for non-aqueous lithium-oxygen batteries *J. Power Sources* **2016**, *331*, 82-90.
10. Liu, B.; Yan, P.; Xu, W.; Zheng, J.; He, Y.; Luo, L.; Bowden, M. E.; Wang, C. M.; Zhang, J. G. Electrochemically formed ultrafine metal oxide nanocatalysts for high-performance lithium- oxygen batteries *Nano Lett.* **2016**, *16*, 4932-4939.
11. Wu, D.; Guo, Z.; Yin, X.; Pang, Q.; Tu, B.; Zhang, L.; Wang, Y. G.; Li, Q. Metal-organic frameworks as cathode materials for Li-O_2 batteries *Adv. Mater.* **2014**, *26*, 3258-3262.
12. Luo, X.; Piernavieja-Hermida, M.; Lu, J.; Wu, T.; Wen, J.; Ren, Y.; Miller, D.; Zak Fang, Z.; Lei, Y.; Amine, K. Pd nanoparticles on ZnO-passivated porous carbon by atomic layer deposition: an effective electrochemical catalyst for Li-O_2 battery *Nanotechnology* **2015**, *26*, 164003.
13. Luo, W. B.; Gao, X. W.; Shi, D. Q.; Chou, S. L.; Wang, J. Z.; Liu, H. K. Binder-free and carbon-free 3D porous air electrode for Li-O_2 batteries with high efficiency, high capacity, and long life, *Small* **2016**, *12*, 3031-3038.
14. Riaz, A.; Jung, K. N.; Chang, W.; Shin, K. H.; Lee, J. W. Carbon-, binder-, and precious metal-free cathodes for non-aqueous lithium-Oxygen batteries: nanoflake-decorated nanoneedle oxide arrays *ACS Appl. Mater. Interfaces* **2014**, *6*, 17815-17822.
15. Zhao, G.; Mo, R.; Wang, B.; Zhang, L.; Sun, K. Enhanced cyclability of Li-O_2 batteries based on TiO_2 supported cathodes with no carbon or binder *Chem. Mat.* **2014**, *26*, 2551-2556.

16. McCloskey, B. D.; Bethune, D. S.; Shelby, R. M.; Mori, T.; Scheffler, R.; Speidel, A.; Sherwood, M.; Luntz, A. C. Limitations in rechargeability of Li-O_2 batteries and possible origins *J. Phys. Chem. Lett*. **2012**, *3 (20)*, 3043-3047.
17. Freunberger, S. A.; Chen, Y.; Peng, Z.; Griffin, J. M.; Hardwick, L. J.; Bardé, F.; Novák, P.; Bruce, P. G. Reactions in the rechargeable lithium-O_2 battery with alkyl carbonate electrolytes *J. Am. Chem. Soc.* **2011**, *133*, 8040-8047.
18. Peng, Z.; Freunberger, S. A.; Chen, Y.; Bruce, P. G. A reversible and higher-rate Li-O_2 battery *Science* **2012**, *337*, 563.
19. McCloskey, B. D.; Speidel, A.; Scheffer, R.; Miller, D. C.; Viswanathan, V.; Hummelshoj, J. S.; Norskov, J. K.; Luntz, A. C. Twin Problems of Interfacial Carbonate Formation in Nonaqueous Li−O_2 Batteries *J. Phys. Chem. Lett.* **2012**, *3*, 997-1001.
20. Sharon, D.; Hirshberg, D.; Afri, M.; Frimer, A. A.; Aurbach, D. The importance of solvent selection in Li–O_2 cells *Chem. Commun.* **2017**, *53*, 3269-3272.
21. Veith, G. M.; Nanda, J.; Delmau, L. H.; Dudney, N. J. Influence of lithium salts on the discharge chemistry of Li-Air cells *J. Phys. Chem. Lett*. **2012**, *3(10)*, 1242-1247.
22. Walker, W.; Giordani, V.; Uddin, J.; Bryantsev, V. S.; Chase, G. V.; Addison, D. A Rechargeable Li-O_2 battery using a lithium nitrate/N,N dimethylacetamide electrolyte *J. Am. Chem. Soc.* **2013**, *135(6)*, 2076-2079.
23. Nasybulin, E.; Xu, W.; Engelhard, M. H.; Nie, Z.; Burton, S. D.; Cosimbescu, L.; Gross, M. E.; Zhang, J. G. Effects of electrolyte salts on the performance of Li-O_2 batteries *J. Phys. Chem. C* **2013**, *117*, 2635-2645.
24. Gao, X.; Chen, Y.; Johnson, L.; Bruce, P. G. Promoting solution phase discharge in Li-O_2 batteries containing weakly solvating electrolyte solutions *Nat. Mat.* **2016**, *15*, 882.
25. Adams, B. D.; Black, R.; Williams, Z.; Fernandes, R.; Cuisinier, M.; Berg, E. J.; Novak, P.; Murphy, G. K.; Nazar, L. F. Towards a stable organic electrolyte for the lithium oxygen battery *Adv. Energy Mater.* **2015**, *5*, 1400867.

26. Nicotera, I.; Oliviero, C.; Henderson, W. A.; Appetecchi, G. B.; Passerini, S. NMR investigation of ionic liquid-LiX mixtures: pyrrolidinium cations and $TFSI^-$ anions *J. Phys. Chem. B* **2005**, *109*, 22814.

27. Zhu, X.; Zhao, T.; Tan, P.; Wei, Z.; Wu, M. A high-performance solid-state lithium-oxygen battery with a ceramic-carbon nanostructured electrode *Nano Energy* **2016**, *26*, 565-576.

28. Léon, A.; Fiedler, A.; Blum, M.; Benkert, A.; Meyer, F.; Wanli, Y.; Baer, M.; Scheiba, F.; Ehrenberg, H.; Weinhardt, L. et al Valence Electronic Structure of Li_2O_2, Li_2O, Li_2CO_3, and LiOH Probed by Soft X-Ray Emission Spectroscopy *J. Phys. Chem. C* **2017**, *121*, 5460-5466.

29. Blum, M.; Weinhardt, L.; Fuchs, O.; Bär, M.; Zhang, Y.; Weigand, M.; Krause, S.; Pookpanratana, S.; Hofmann, T.; Yang, W. et al Solid and liquid spectroscopic analysis (SALSA) - a soft x-ray spectroscopy endstation with a novel flow-through liquid cell *Rev. Sci. Instrum.* **2009**, *80*, 123102.

30. Fuchs, O.; Weinhardt, L.; Blum, M.; Weigand, M.; Umbach, E.; Bär, M.; Heske, C.; Denlinger, J. D.; Chuang, Y. D.; McKinney, W. et al High-resolution, high-transmission soft x-ray spectrometer for the study of biological samples *Rev. Sci. Instrum.* **2009**, *80 (6)*, 063103.

31. Kato, M.; Morishita, Y.; Oura, M.; Yamaoka, H.; Tamenori, Y.; Okada, K.; Matsudo, T.; Gejo; T., Suzuki, I. H.; Saito, N. Absolute photoionization cross sections with ultra-high energy resolution for Ar, Kr, Xe and N_2 in inner-shell ionization regions J. Electron Spectrosc. Relat. Phenom. **2007**, *160*, 39-48.

32. Lusvardi, V. S.; Barteau, M. A.; Chen, J. G.; Eng, J.; Frühberger, B.; Teplyakov, A. An NEXAFS investigation of the reduction and reoxidation of TiO_2(001) *Surf. Sci.* **1998**, *397*, 237-250.

33. Kanai, K.; Nishi, T.; Iwahashi, T.; Ouchi, Y.; Seki, K.; Harada, Y.; Shin, S. Electronic structures of imidazolium-based ionic liquids, J. Electron Spectrosc. Relat. Phenom. **2009**, *174*, 110-115.

34. Howlett, P. C.; Izgorodina, E. I.; Forsyth, M.; MacFarlane, D. R. Electrochemistry at negative potentials in bis(trifluoromethanesulfonyl) amide ionic liquids *Z. Phys. Chem.* **2006**, *220*, 483-1498.

35. Ong, S. P.; Andreussi, O.; Wu, Y.; Marzari, N.; Ceder, G. Electrochemical windows of room-temperature ionic liquids from molecular dynamics and density functional theory calculations *Chem. Mater.* **2011**, *23*, 2979-2986.

36. Nishino, S.; Fujiwara, T.; Yamasaki, H.; Yamamoto, S.; Hoshi, T. Electronic structure calculations and quantum molecular dynamics simulations of the ionic liquid PP13-TFSI *Solid State Ion.* **2012**, *225*, 22-25.

37. Olivares-Marin, M., Sorrentino, A.; Pereiro, E.; Tonti, D. Discharge products of ionic liquid-based Li-O_2 batteries observed by energy dependent soft x-ray transmission microscopy *J. Power Sources* **2017**, *359*, 234-241.

Figure captions

Figure 1. Cyclic voltammetry curve of Li/PP13(TFSI) + 0.5M LiTFSI/C (scan rate of 10 mV s^{-1}), using an argon flow (green curve, one cycle), followed by an oxygen flow (red, two cycles). For further *ex situ* analysis of the cathodes, the electrochemical reaction was stopped at potentials V_1 and V_2 during the discharge, and at potentials V_3 and V_4 during the charging of the Li-O_2 cell.

Figure 2. N K XES spectra of the electrolyte (red), the salt (LiTFSI, blue), and the solvent PP13(TFSI) (purple). The spectrum labeled "PP13" shows the weighted difference of the solvent and salt spectra, as calculated by the equation given below the molecular structures.

Figure 3. N K XES spectra (red circles) after stopping at the four potentials described in Figure 1, together with the corresponding two-component fits (solid black lines) using PP13(TFSI) (purple lines) and LiTFSI (blue lines), as well as the corresponding residuals.

Figure 4. Evolution of the relative spectral contribution of the PP13(TFSI) and LiTFSI components to the N K spectra of the electrolyte during the first cycle.

Figure 5: (a) O K XES spectra of the cathode electrode as received ("GDL"), the electrolyte as prepared ("Electrolyte"), and the cathode after discharge at potential V_2. (b) O K XES spectrum of the cathode after stopping at potential V_2 (red dots) and the corresponding fit (black) using three components (i.e., GDL, electrolyte, and lithium peroxide). Below the fit, three magnified (x10) residuals are shown: for the three-component fit ("V_2-fit residual") and for the four-component fits "adding LiOH" and "adding $LiCO_3$", respectively. The spectra of the three reference compounds are also shown.

Figure 6. Schematic view of the novel flow-through electrochemical cell, designed for *ex-situ, in-situ, and operando* XES measurements with the SALSA endstation (SS: stainless steel, PEEK: polyether ether ketone).

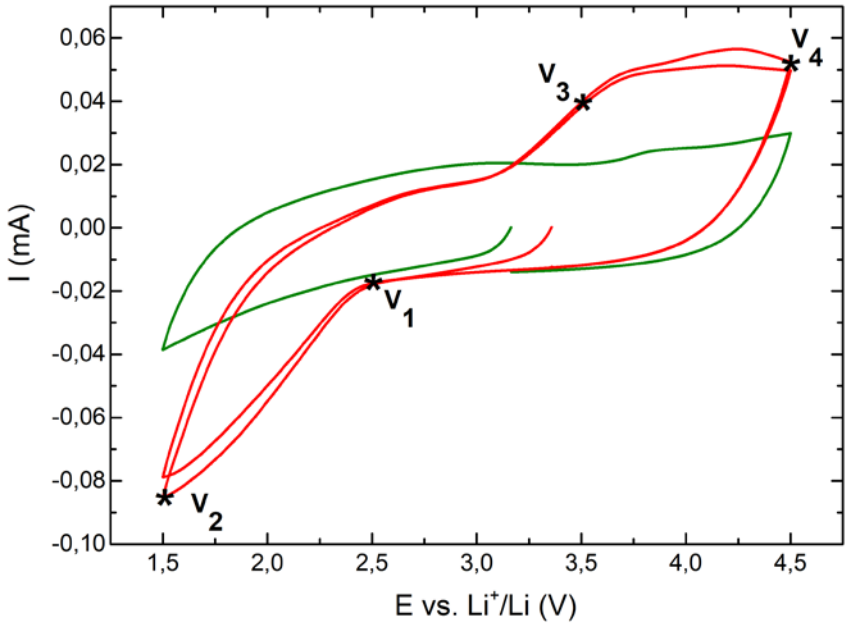
0,06
0,04
0,02
0,00
-0,02
-0,04
-0,06
-0,08
-0,10
I (mA)
1,5
2,0
2,5
3,0
3,5
4,0
4,5
E vs. Li+/Li (V)
V1
V2
V3
V4

Figure 1

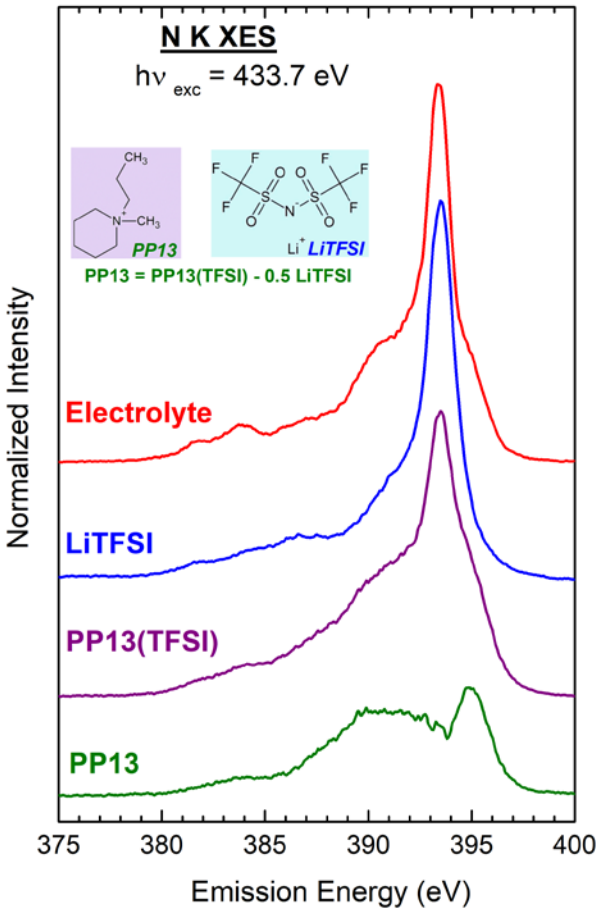
N K XES
hν exc = 433.7 eV
PP13
Li+ LiTFSI
PP13 = PP13(TFSI) - 0.5 LiTFSI
Electrolyte
LiTFSI
PP13(TFSI)
PP13
Normalized Intensity
375
380
385
390
395
400
Emission Energy (eV)

Figure 2

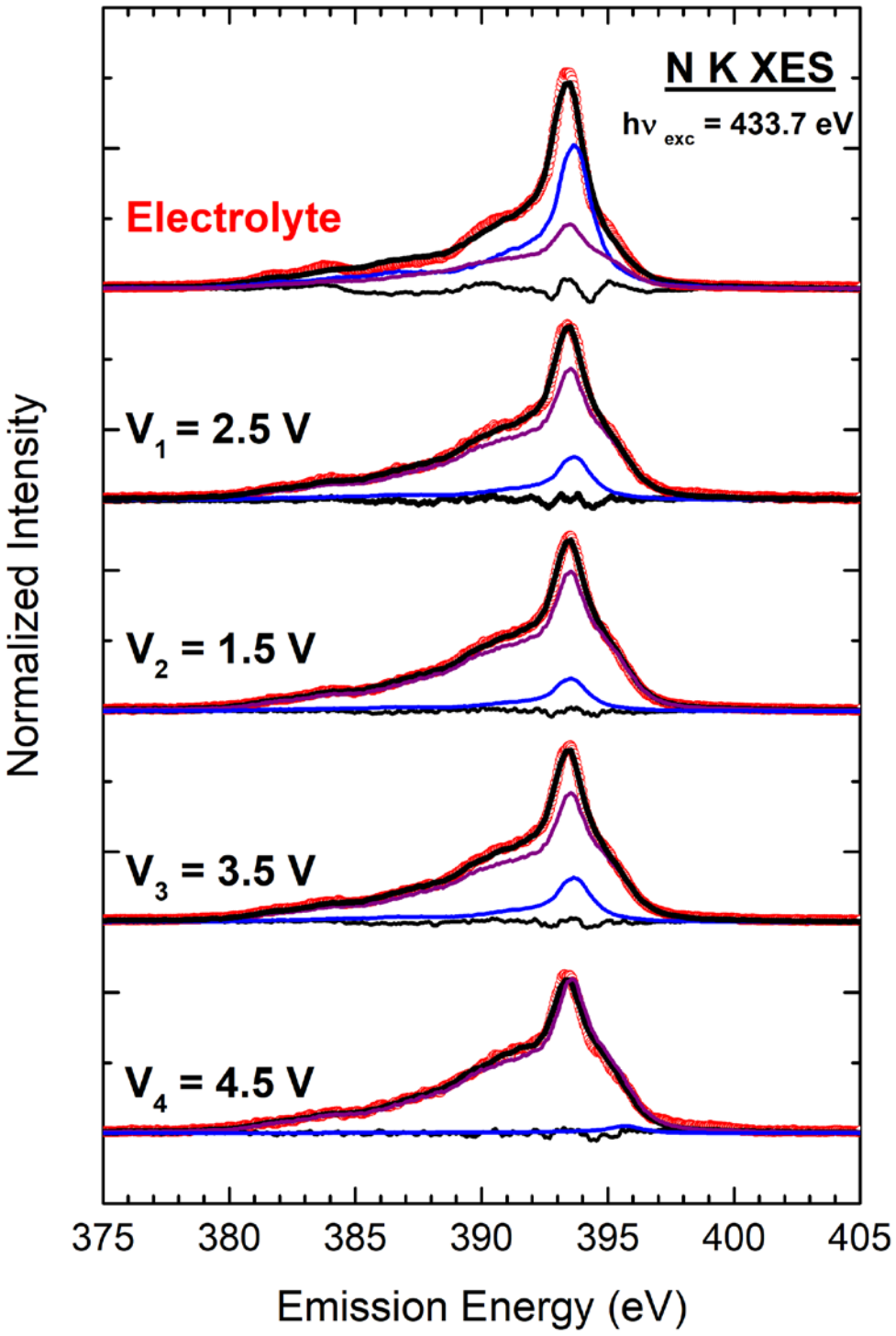
N K XES
hν exc = 433.7 eV
Electrolyte
V1 = 2.5 V
V2 = 1.5 V
V3 = 3.5 V
V4 = 4.5 V
Normalized Intensity
375
380
385
390
395
400
405
Emission Energy (eV)

Figure 3

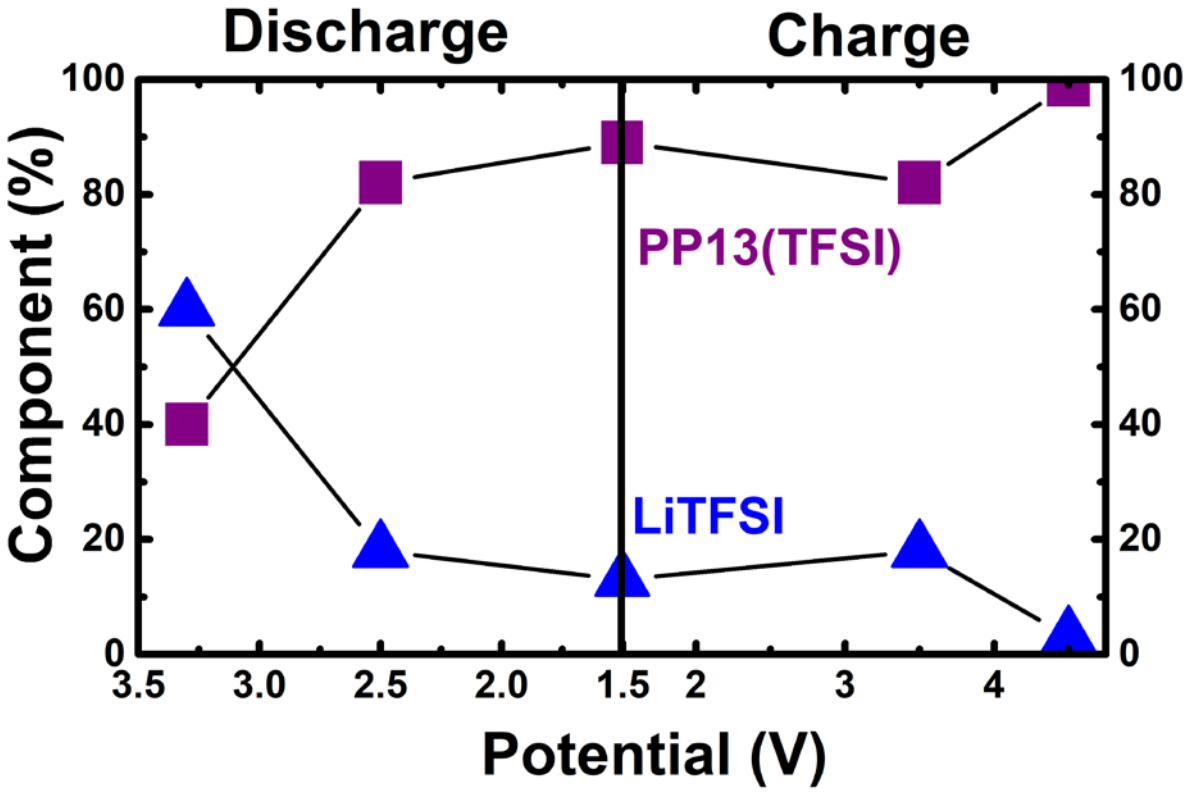
Discharge
Charge
Component (%)
100
80
60
40
20
0
PP13(TFSI)
LiTFSI
3.5
3.0
2.5
2.0
1.5
2
3
4
Potential (V)

Figure 4

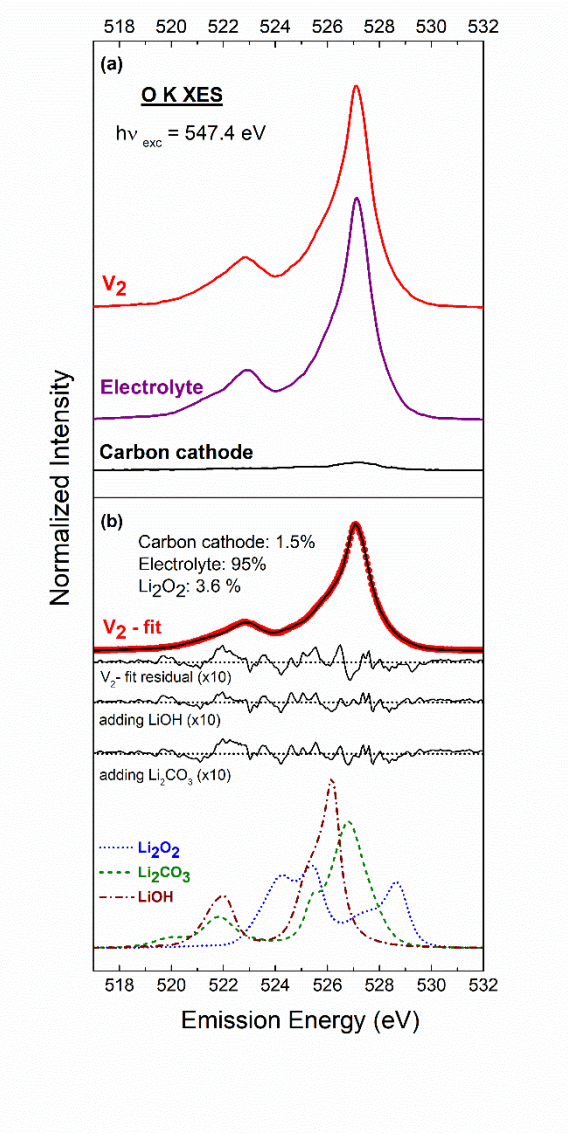
518 520 522 524 526 528 530 532
(a)
O K XES
hν exc = 547.4 eV
V2
Electrolyte
Carbon cathode
(b)
Carbon cathode: 1.5%
Electrolyte: 95%
Li2O2: 3.6 %
V2 - fit
V2- fit residual (x10)
adding LiOH (x10)
adding Li2CO3 (x10)
Li2O2
Li2CO3
LiOH
Normalized Intensity
Emission Energy (eV)

Figure 5

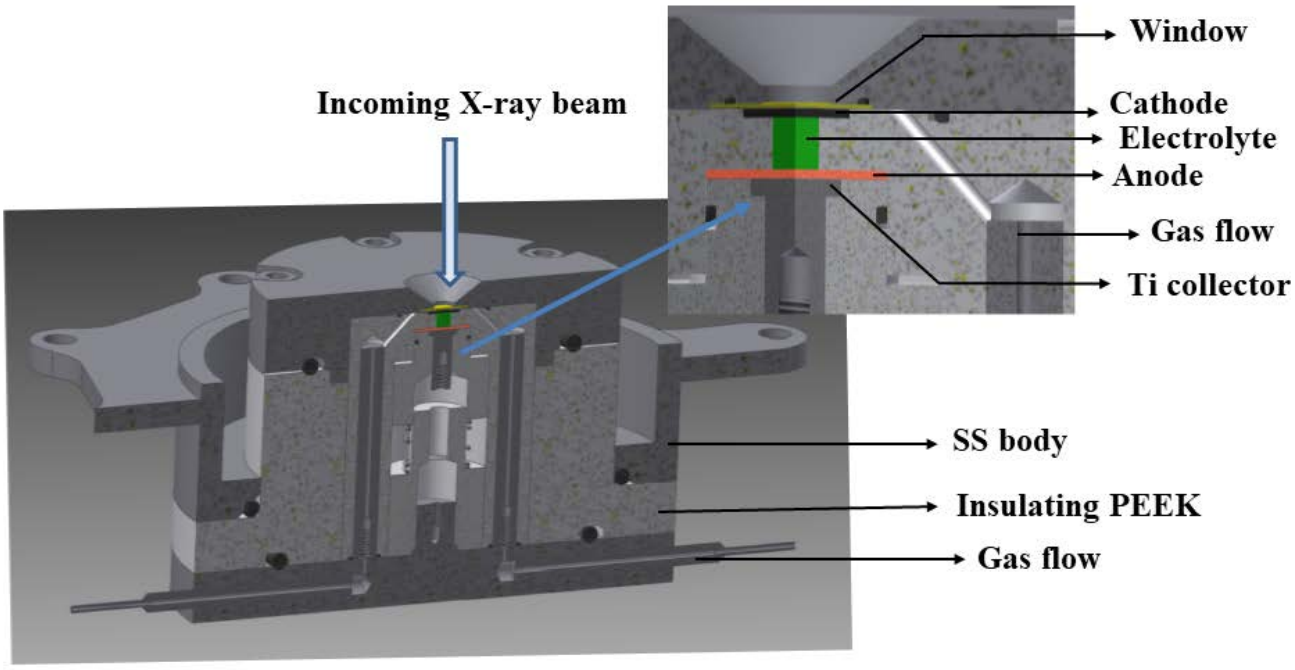
Incoming X-ray beam
Window
Cathode
Electrolyte
Anode
Gas flow
Ti collector
SS body
Insulating PEEK
Gas flow

Figure 6

TOC Graphic